Perspective

Capillary forces generated by biomolecular condensates

https://doi.org/10.1038/s41586-022-05138-6

Received: 28 August 2021

Accepted: 25 July 2022

Published online: 7 September 2022

Check for updates

Bernardo Gouveia[1,6], Yoonji Kim[2,6], Joshua W. Shaevitz[3], Sabine Petry[2], Howard A. Stone[4]✉ & Clifford P. Brangwynne[1,5]✉

Liquid–liquid phase separation and related phase transitions have emerged as generic mechanisms in living cells for the formation of membraneless compartments or biomolecular condensates. The surface between two immiscible phases has an interfacial tension, generating capillary forces that can perform work on the surrounding environment. Here we present the physical principles of capillarity, including examples of how capillary forces structure multiphase condensates and remodel biological substrates. As with other mechanisms of intracellular force generation, for example, molecular motors, capillary forces can influence biological processes. Identifying the biomolecular determinants of condensate capillarity represents an exciting frontier, bridging soft matter physics and cell biology.

The intracellular environment is a complex and crowded sea of biomolecules, buffeted by incessant motion from Brownian thermal fluctuations and biological activity. Cellular function is achieved by bringing order to this environment, in large part through subcompartmentalization into a spatially controlled and compositionally defined organization. Historically, these compartments were thought of almost exclusively as membrane-bound structures, but recent work has highlighted the importance of membraneless organelles, also known as biomolecular condensates, which form through phase transitions, including liquid–liquid phase separation[1,2]. Some of the dozens of examples of such protein and nucleic acid-rich condensates include P granules[3,4], nucleoli[5,6], stress granules[7], the pyrenoid[8] and DNA repair foci[9]. Multivalent interactions, generally mediated by repetitive biomolecular motifs[10], including sequence-patterned prion-like or intrinsically disordered proteins[11], drive the formation of condensates. These are important for diverse functional roles, generally by locally increasing the concentration of specific biomolecules by 100-fold or more.

Most studies to date have focused on the role of condensates as biomolecular compartments. However, an underappreciated feature of these condensates is that they can form interfaces with the cytoplasm, other condensates and cellular structures around them. These interfaces lead to capillary, or interfacial, forces. In non-living soft matter systems, such interfaces have important organizational roles, for example, in defining the topologies of multiphase liquids[12] or shaping the geometry of soft materials[13–15]. Capillary forces are also present in everyday phenomena such as the breakup of a stream of faucet water into individual droplets, the attraction of cereal sitting on the surface of a bowl of milk, or the droplets that form on the vertical sides of a glass of wine.

Capillary forces have been widely suggested to have important roles in multicellular tissue organization[16,17], but the role of capillarity within living cells has been relatively unexplored. The recent recognition that liquid-like biomolecular condensates are ubiquitous within living cells highlights a plethora of new liquid–liquid and liquid–solid interfaces through which capillary forces can act to reorganize and localize intracellular materials and their substrates. Indeed, the interface between one condensate and another or with a solid or deformable substrate, such as a membrane, can be a site of force generation. The same thermodynamic driving forces that promote phase separation can also lead to capillary forces that do mechanical work, impacting the local mechanics, morphology, organization and function of condensates.

The role of intracellular capillarity is only now emerging but is becoming increasingly clear. Elucidating the molecular origins and consequences of capillary phenomena will open up new qualitative and quantitative frameworks for understanding the structure, organization and function of living cells. Although many of the studies that we discuss make no explicit mention of capillarity, it likely represents a key aspect of the underlying physics.

Fundamental principles of capillary phenomena

To understand how force-generating interfaces are formed, we first consider the simplest equilibrium thermodynamic model for phase separation. The Flory–Huggins model provides a mean-field expression for the free energy of mixing Δf in a polymer–solvent system[18]. Two ideal, non-interacting species will mix, as doing so maximizes their configurational entropy. The Flory–Huggins model makes two corrections to this purely entropic picture[18]. First, the connectivity of the polymer constrains its allowed configurations, reducing the entropy in a way that scales with the polymer length. Second, energetic interactions are captured through the χ parameter, which encodes how much the two components favour homotypic, for example, polymer–polymer and solvent–solvent, interactions compared with heterotypic, for example, polymer–solvent, interactions. The greater the value of χ, the stronger the driving force is for phase separation (Box 1 Fig. panel **a**).

Once phase separation occurs and a new surface is created, there is an associated interfacial tension. Inside the condensate bulk, each molecule

[1]Department of Chemical and Biological Engineering, Princeton University, Princeton, NJ, USA. [2]Department of Molecular Biology, Princeton University, Princeton, NJ, USA. [3]Department of Physics, Princeton University, Princeton, NJ, USA. [4]Department of Mechanical and Aerospace Engineering, Princeton University, Princeton, NJ, USA. [5]The Howard Hughes Medical Institute, Princeton, NJ, USA. [6]These authors contributed equally: Bernardo Gouveia, Yoonji Kim. ✉e-mail: hastone@princeton.edu; cbrangwy@princeton.edu

Box 1

Fundamentals of phase separation

a, Flory–Huggins free energy $\Delta f/k_BT = (\phi/P)\log\phi + (1-\phi)\log(1-\phi) + \chi\phi(1-\phi)$ plotted versus polymer volume fraction ϕ for different values of χ for degree of polymerization P=1. Phase separation occurs if the system is in the shaded region above the critical point (black star), in which the green colouring represents polymer-rich concentrations and the blue colouring represents solvent-rich concentrations. The binodal denotes the lowest common tangent of the free energy curve and gives the compositions of the dense and dilute phases. The spinodal delineates the limit of system metastability. **b**, Individual macromolecules (green squiggly lines) must come together to form a microscopic cluster of radius > R^* to initiate phase separation. **c**, Coarsening processes act to reduce the total interfacial area. Coalescence involves two droplets merging to form a larger droplet. Ostwald ripening involves a small droplet dissolving due to capillary pressure and the resulting molecules diffusing into a larger droplet. **d**, In the absence of additional processes, phase separation ends with a single large polymer-rich droplet of radius R suspended in the solvent-rich phase with interfacial tension γ.

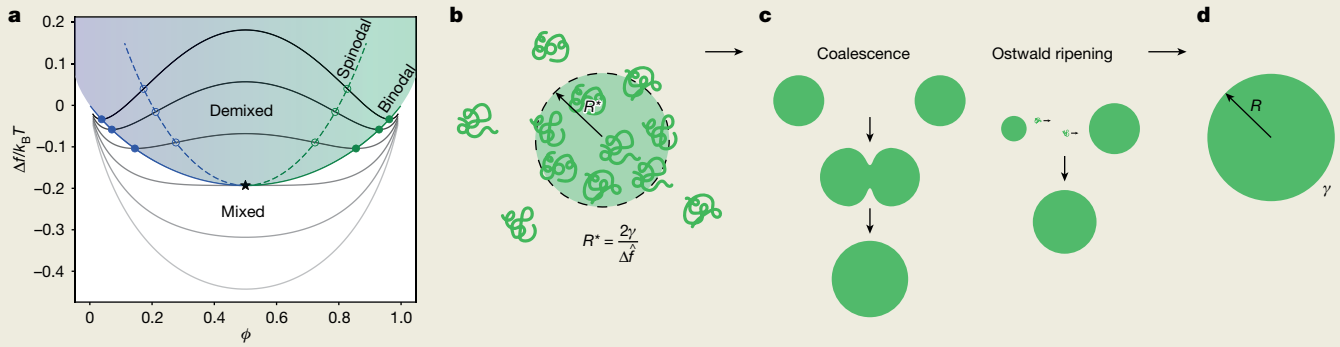

shares a cohesive energy $u = n\epsilon/2$ on average with its n neighbours (Box 2 Fig. panel **a**), where ϵ is the typical energy scale of molecular interactions. However, molecules at the interface miss out on roughly half of these interactions and pay a penalty $\Delta u = n\epsilon/4$. Thus, molecules energetically prefer to be in the bulk of the condensate, even though some must necessarily reside at the interface. This frustration experienced by surface molecules is the origin of interfacial tension γ, which represents the energy penalty per unit area of interface. For a molecule of typical linear size a, for example, the radius of gyration of a polymer, the area per molecule scales approximately a^2, so the interfacial tension is given by

$$\gamma \approx \Delta u/a^2 \approx n\epsilon/4a^2. \quad (1)$$

Equation (1) demonstrates that interfacial tension increases with stronger attractive energy and decreases with the square of the molecular size[19]. It costs free energy to increase the surface area ΔA of an interface, that is, $\Delta F = \gamma\Delta A$, so condensates decrease this free energy by minimizing surface area.

Within the Flory–Huggins framework, the interfacial tension in a binary phase-separated mixture is given by $\gamma \approx k_BT\chi/a^2$ (ref. [20]). An interface implies a sharp compositional discontinuity—the energetics of which are precisely what χ encodes. We note that most practical calculations used to study phase-separated interfaces are performed using a phase-field approach, such as the Cahn–Hilliard model[21–23].

From a mechanical perspective, interfacial tension manifests as a force per unit length. Intuitively, we are familiar with how rapidly a soap bubble disintegrates when ruptured—this is due to the interface being under tension. This tension at the interface has a profound effect on the state of stress, for example, pressure or force per unit area, of the condensate compared with the stress of the surrounding bulk. In particular, for a static spherical droplet of radius R, the hydrostatic pressure difference between the condensate and the bulk is given by

$$\Delta p = 2\gamma/R, \quad (2)$$

which is referred to as the capillary pressure (Box 2 Fig. panel **b**). Intuitively, smaller droplets, which have higher curvatures, are in a state of greater pressure than the surrounding fluid.

In a sample of phase-separated droplets, that is, an emulsion, interfacial tension continually acts to minimize the total condensate surface area, favouring a smaller number of larger droplets. Such coarsening behaviour commonly occurs through two mechanisms: droplet coalescence and Ostwald ripening (Box 1 Fig. panel **c**). Droplet coalescence involves two condensates finding each other and merging to form a single larger droplet with a smaller total surface area. The speed that droplets coalesce is roughly set by the capillary velocity γ/μ, where μ is the condensate viscosity, although more realistic models of condensate rheology will affect this estimate[5,24–28]. Ostwald ripening occurs when a small droplet dissolves and the molecules that composed it diffuse into a larger droplet—a direct consequence of the larger capillary pressure (equation (2)) of the smaller droplet.

Because interfacial dynamics also depend on the stress difference between the bulk surroundings and the condensate, the rheological properties of the surrounding cytoplasm or nucleoplasm can also impact coarsening dynamics. For example, if the viscosity of the surrounding environment μ_{env} is higher than that of the condensate, it will tend to dominate the coalescence timescale, and the relevant capillary velocity would be γ/μ_{env} (ref. [29]). Moreover, if the bulk exhibits spatially varying stiffness, condensates are likely to dissolve in regions of high stiffness to re-form in less stiff regions[30]. This so-called elastic ripening acts synergistically with Ostwald ripening and can even produce faster coarsening depending on how the magnitude of the stiffness gradient compares with the interfacial tension.

Capillary forces at intracellular liquid interfaces

As the above discussion makes clear, capillary forces are driven by interfaces, including those between a condensate and another immiscible liquid or a solid. In such 'wetting' phenomena, there are three

Box 2

Fundamentals of capillarity

a, Microscopic definition of interfacial tension γ as an energy penalty per unit area. Condensate molecules are shown as green squiggles and are of typical size a. ϵ is the typical attractive energy scale between condensate molecules and n is the number of neighbours each molecule can interact with. γ scales inversely with the square of molecular size a and proportionally with the strength of the attractive energy ϵ (equation (1)). **b**, Macroscopic definition of γ as a tensile force per unit length that acts to try and flatten area elements, that is, minimize area. The arrows denote the area element under tension. For a quiescent spherical condensate, the pressure inside the condensate p_B is higher than the surrounding pressure p by an amount $2\gamma/R$, which is called the capillary pressure. **c**, Condensates can either totally wet a substrate, forming a coating, or can partially wet a substrate, forming an approximately spherical cap with contact angle θ. **d**, A droplet of radius R that is mostly wetting to a membrane will pull it upwards with a capillary torque $\approx 2\pi\gamma R^2$, with the moment arm shown by the dotted line, which will be resisted by the bending stiffness κ. This deforms the membrane on a length scale $\approx l_{ec} = \sqrt{\kappa/\gamma}$, with radius of curvature shown by the dotted circle, so as to maximize contact with the membrane while minimizing the bending energy. **e**, Adhesive forces due to capillary bridges formed between two planar substrates and between a sphere and a plane. Remarkably, the latter has a force independent of the condensate volume. **f**, A particle of radius R that partially wets an interface will always adhere to the interface, even if $\gamma_{SB} < \gamma_{SC}$, as the total interfacial energy is changed by an amount $E_{wet} = -\gamma\pi R^2(1-\cos\theta)^2$, which is always negative. This is the basis for the stability of Pickering emulsions.

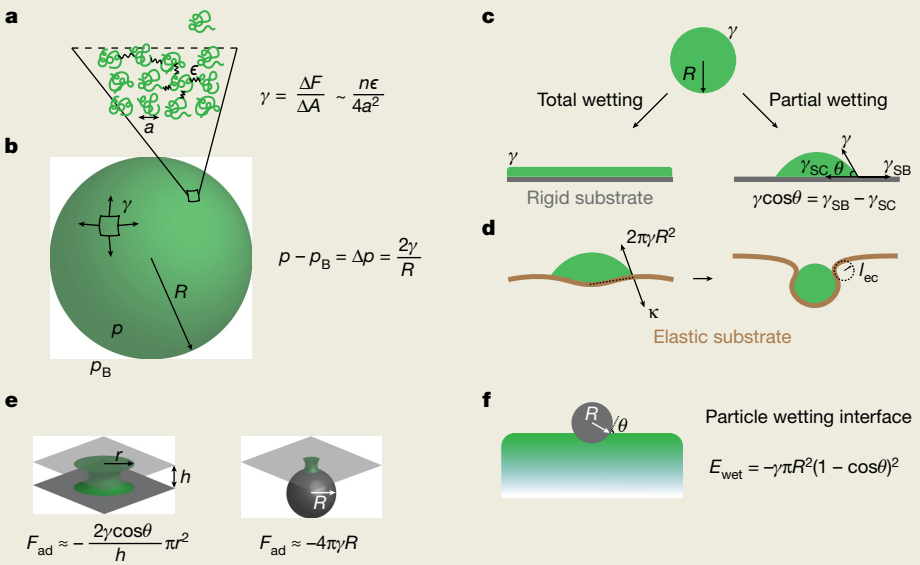

interfacial tensions at play: (1) the condensate–bulk γ, (2) the substrate–condensate γ_{SC}, and (3) the substrate–bulk γ_{SB}. As interfaces with the highest tension pay the largest energy penalty, their area is minimized. For example, if the interfacial energy associated with the condensate wetting the substrate $\gamma + \gamma_{SC}$ is lower than that of the substrate–bulk γ_{SB}, then the latter interface is eliminated with the condensate totally coating the substrate (Box 2 Fig. panel **c**). However, intermediate cases also occur, in which droplets can partially wet the substrate, forming an approximately spherical cap defined by a contact angle θ that satisfies a tangential force balance at the contact line (Box 2 Fig. panel **c**).

Perhaps the most well-known examples of intracellular wetting phenomena are biomolecular condensates wetting other condensates, as seen in multiphase droplets, such as nucleoli, stress granules and nuclear speckles[5,31,32] (Fig. 1). On the basis of in vitro data and experiments conducted in living cells, the structure of multiphase condensates appears to reflect their compartmentalized functions. For example, transcription and splicing are thought to occur in the 'shell' region of nuclear speckles, whereas the 'core' is important for RNA maturation[32]. The clearest example of such core–shell architecture is in the multilayering of the nucleolus (Fig. 1c), which exhibits three distinct membraneless liquid-like subcompartments[5]. The different interfacial tensions between each subcompartment are thought to determine how the three immiscible phases are organized, as has also been recently examined in model RNA and polypeptide systems[33–35] (Fig. 1b) and elastin-like polyproteins[36]. In the case of the nucleolus, the resulting core–shell architecture enables carrying out specific functions important for the sequential assembly of pre-ribosomal particles[5] (Fig. 1c).

Several other examples of liquid–liquid wetting behaviour are observed in cells, although in most cases, little is known about their biophysical origins or relevance to biological function. For example, Cajal bodies wetting snurposomes are seen in the *Xenopus* germinal vesicle[37] (Fig. 1d). In other systems, Cajal bodies interact with nucleoli, as shown by electron micrographs of Cajal bodies tethered to the nucleolar surface in rat trigeminal ganglion neurons[38]. Stress granules and P bodies are two types of condensates that are associated with translational regulation of cytoplasmic mRNA transcripts, which are released from polysomes under cellular stress, for example, oxidative stress upon sodium arsenite treatment. Despite being compositionally related with many shared components, they are distinct and immiscible with one another, even while remaining physically juxtaposed (Fig. 1e). A recent study using a U2OS cell culture model has found that this multiphase coexistence depends on the stoichiometry of key stress granule and P body components[31], although the biophysical determinants of this immiscibility and the role of the relative interfacial

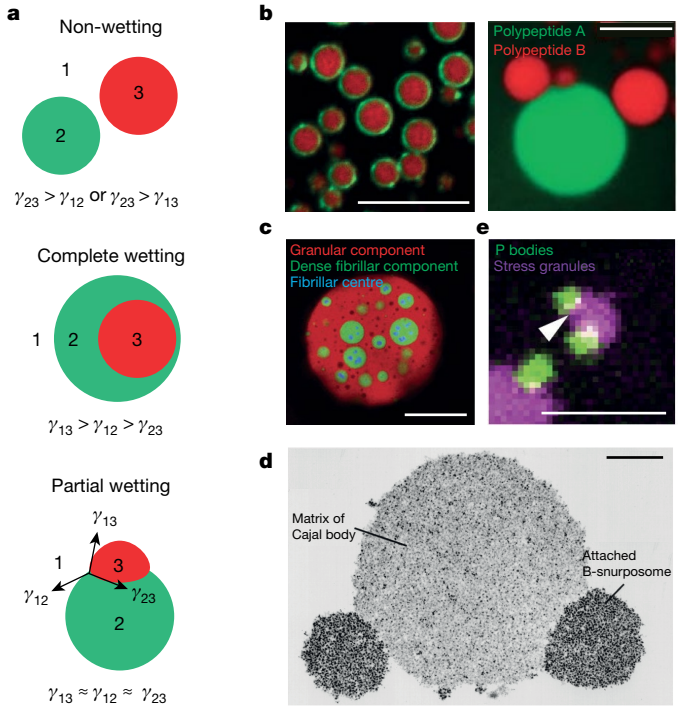

Fig. 1 | Examples of capillarity in multiphase condensate organization. **a**, Different modes of multiphase droplet structuring due to relative interfacial tensions. **b**, The Ewing sarcoma (EWS) prion-like polypeptide (green) completely wets the surface of the arginine-rich polypeptide–RNA droplets (red) at low RNA concentration (left). Scale bar, 10 µm. Partial wetting behaviour shown by the prion-like polypeptide droplet (polypeptide A in green) and two RRP–RNA droplets (polypeptide B in red) (right). Scale bar, 10 µm. Images modified from ref. [33], CC BY 4.0. **c**, The multilayered nucleolus follows a clearly delineated core–shell structuring due to immiscibility between the different phases, in which each phase facilitates distinct steps in the overall multistep ribosomal assembly process. Nucleoli with the granular component (red), dense fibrillar centre (green) and fibrillar centre (blue) shown in an *X. laevis* germinal vesicle. Scale bar, 20 µm. Image modified with permission from ref. [5]. **d**, Two B-snurposomes wetting a Cajal body in the *X. laevis* germinal vesicle. Scale bar, 1 µm. Image modified with permission from ref. [37]. **e**, P bodies marked by LSM14A (green; white arrowhead) attached to stress granules marked by G3BP1 (purple), resembling partial wetting behaviour. Scale bar, 3 µm. Image modified with permission from ref. [31].

tensions are unclear. In all of these cases, the condensate–condensate interface probably allows for exchange of materials between the two, thereby facilitating sequential biomolecular processing.

To quantitatively understand these surface phenomena, directly measuring interfacial tensions is needed. Several methods have been developed to estimate the interfacial tension of biomolecular condensates, such as measuring droplet coalescence times together with viscosity measurements, capillary fluctuations, wetting contact angles and droplet shapes[5,39,40]. Of note are active microrheological methods utilizing optical trapping[41] or micropipette aspiration[42] of condensed droplets, from which interfacial tensions can be extracted[43]. Quantitative live-cell imaging and optogenetic tools have also been used to probe the material properties of intracellular condensates[44–46] along with methods to induce localized phase separation on specifically targeted genomic regions[47]. Estimates put the value of interfacial tensions of biomolecular condensates in the range of $\gamma \approx 10^{-4}$ to 10^{-7} N m^{-1} (refs. [5,39–41,48]). These interfacial tensions are far smaller than those of air–water interfaces with $\gamma \approx 10^{-1}$ N m^{-1}—a direct consequence of interfacial tension scaling inversely with macromolecular size (equation (1)). However, other macromolecular liquids, such as colloidal systems[19], have comparably small interfacial tensions, which can nonetheless give rise to significant capillary stresses at the nanoscale.

Although efforts to quantify the interfacial properties of nanoscale condensates are only beginning, their effects have been detected recently in the early-stage kinetics of condensate nucleation[48,49]. A droplet of radius R will nucleate only if the driving force for phase separation can overcome the interfacial penalty, set by γ. The sum of these two contributions to the total free energy leads to an energy barrier that selects a minimum stable droplet radius $R^* = 2\gamma/\Delta\hat{f}$ (ref. [50]) (Box 1 Fig. panel **b**), where $\Delta\hat{f}$ is the free energy density difference between the bulk phase and the condensed phase. Thus, interfacial tension introduces a destabilizing energetic barrier, such that assemblies with radius smaller than R^* are unstable and dissolve. A super-resolution microscopy approach indicated the first links to this phase transformation framework by showing that the early stages of protein aggregation are consistent with a critical cluster size[48]. Another recent study examining a combination of endogenous and synthetic intracellular condensates has found a strong dependence of the nucleation rate on the degree of supersaturation and molecular features of nucleation sites, which is another prediction of classical nucleation theory[49].

Capillary forces at soft interfaces

Biomolecular sequences of protein and nucleic acid constituents will tune interfacial tensions underlying condensate-driven capillary forces, but we have few measurements or theoretical frameworks for elucidating this connection. Addressing this gap will be important for developing predictive models of not only the capillary forces that act at liquid–liquid interfaces but also how condensates wet different biological substrates, such as cytoskeletal filaments, membranes, and DNA and RNA (see section Capillary forces and genome organization).

Interactions between condensates and cytoskeletal filaments are a particularly exciting new area, specifically when cytoskeletal components such as actin filaments, microtubules and intermediate filaments impact the assembly (or disassembly), deformation and reorganization of condensates, and vice versa[51–54] (Fig. 2a). As semiflexible rods, cytoskeletal filaments within condensates could give rise to liquid crystalline internal anisotropies with parallels to an existing body of work in the field of orientable active matter[55,56]. For example, concentrated solutions of actin were found to form tactoid-shaped condensates in the presence of the crosslinker filamin[57]. Under certain conditions, cylindrical actin bundles formed that subsequently broke up into a chain of tactoids due to the interfacial Rayleigh–Plateau instability (Fig. 2b). The potential for such structural anisotropies and the role of non-equilibrium activity, for example, chemical reactions[58] or molecular motors[59], in controlling or overcoming capillary forces remain an important but largely unexplored area.

Microtubules are another key cytoskeletal filament and represent the stiffest intracellular biopolymer, with important structural roles, including building the mitotic spindle for cell division. Several microtubule-binding proteins can form microtubule-associated condensates, including BuGZ[60], TPX2 (ref. [61]), tau[62,63] and CLIP170 (ref. [64]). In the case of TPX2 and CLIP170, a uniform condensate film totally wets the microtubule, but a Rayleigh–Plateau instability occurs that breaks up the film into regularly spaced droplets[64,65] (Fig. 2c). TPX2 had been known to initiate branching of microtubules[66], which nucleate directly from these droplets.

Similar wetting behaviour was found for the protein tau, which forms a tubulin-enriching condensate that bundles microtubules[62], probably due to capillary adhesion. Indeed, any time a mostly wetting liquid is sandwiched between two substrates, it forms a capillary bridge that produces an adhesive force, which is given by $F_{wet} = \Delta p A_{wet}$, where A_{wet} is the substrate area wetted by the condensate, and Δp is the capillary pressure difference between the condensate and the bulk. One can estimate the scale of these adhesive bundling forces using the formula in Box 2 Fig. panel **e**: with $\gamma \approx 10^{-5}$ N m^{-1}, the adhesive force holding two 1-µm-long microtubules a diameter apart is $F_{wet} \approx 10$ pN. Remarkably,

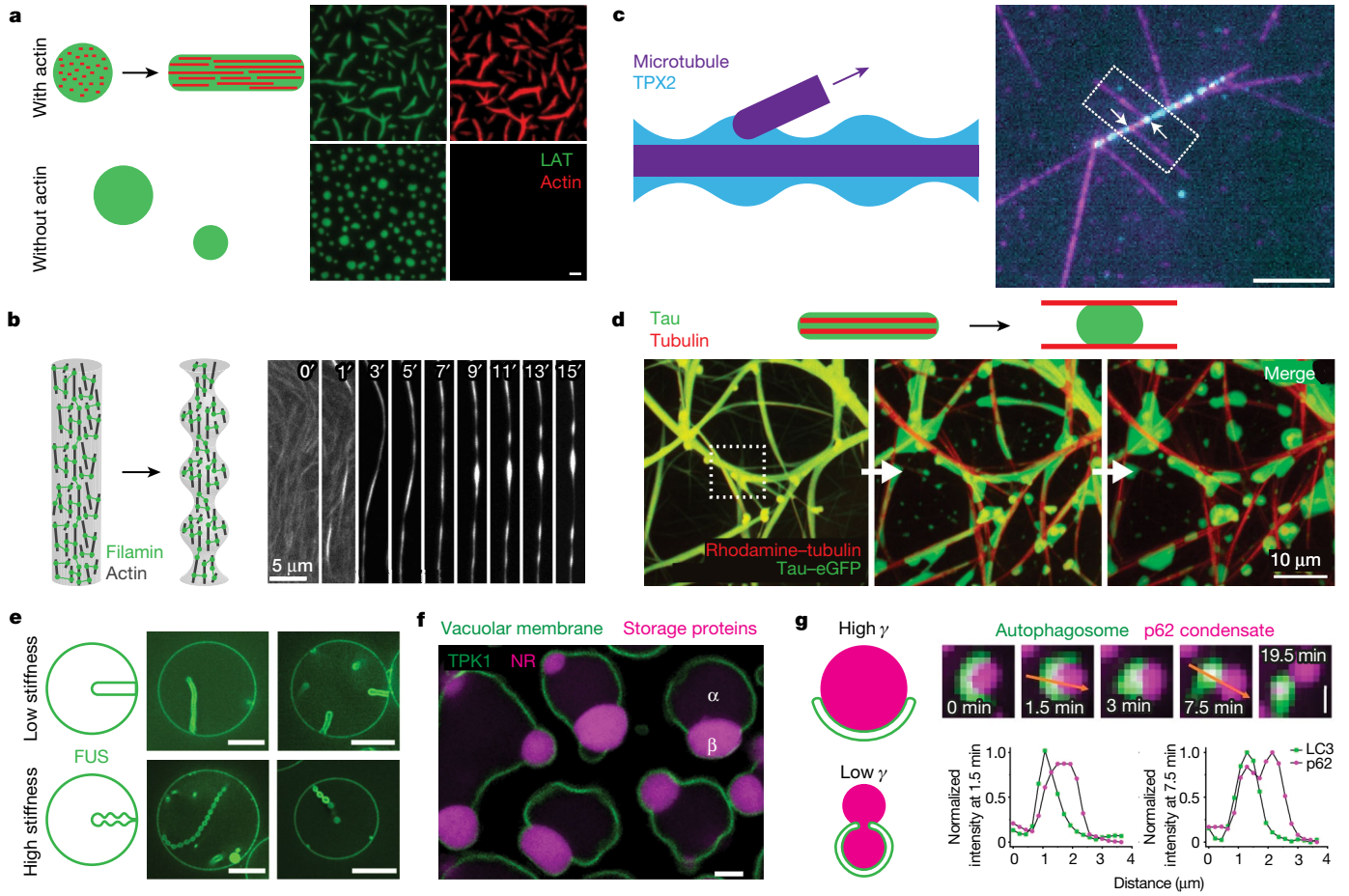

Fig. 2 | Capillarity on substrates. a, Linker for activation of T cells (LAT) condensates promote actin polymerization, which leads to subsequent deformation of the condensates. Scale bar, 2 μm. Image reproduced with permission from ref. [52]. **b**, Actin condensing into a cylindrical thread due to filamin crosslinking. Interfacial tension causes the thread to break up into an array of tactoids via the Rayleigh–Plateau instability. Image reproduced with permission from ref. [57]. Time is measured in minutes. **c**, Condensed TPX2 forms droplets along microtubules due to the Rayleigh–Plateau instability. These droplets recruit additional factors that nucleate microtubule branches, with examples shown in the dotted box. Image reproduced from ref. [65]. Scale bar, 5 μm. **d**, Condensed tau wets microtubules and bundles them. This interaction can be tuned by adding heparin, which induces a dewetting transition. The dotted box shows a region where microtubule unbundling is clear. White arrows show the passage of time from 0 to 60 min. Image reproduced from ref. [62] CC BY-NC-ND 4.0. **e**, Fused in sarcoma (FUS) condenses on lipid membranes and exerts compressive stresses that lead to inward pointing tubules. The higher the bending stiffness of the membrane, the more likely pearled tubules are to form. Image reproduced with permission from ref. [72]. Scale bars, 5 μm. **f**, Phase-separated droplets containing storage proteins stained by neutral red (NR) wet and deform the vacuolar membrane, eventually budding out to form protein storage vacuoles. Scale bar, 2.5 μm. Image reproduced from ref. [75], CC BY 4.0. **g**, Time course showing a LC3-labelled autophagosome forming to encapsulate a p62 droplet. Image reproduced from ref. [74]. The orange arrows show the distances over which the fluorescence intensities below are plotted. Autophagosomes can only form if the interfacial tension of p62 condensates is sufficiently low. Scale bar, 1 μm.

this force scale is similar to that applied by conventional molecular motors[67] that crosslink and apply forces to microtubules.

By adding the molecule heparin to disrupt the tau–tubulin interaction, condensed tau was observed to dewet from these bundles (Fig. 2d). Another study has shown that microtubule regions coated with condensed tau protected them from microtubule-degrading enzymes, but processive molecular motors such as kinesin 8 were able to penetrate these condensed tau regions, resulting in their dissolution[62,63]. This raises the question of how a molecular motor responds when it runs into the contact line defining the microtubule–condensate interface. More generally, because of the prominent importance of tau in neurodegenerative diseases, this area of study represents a fascinating intersection emerging between capillary phenomena and pathology[68–70].

Membranes present yet another surface where condensates can exert capillary forces, with wetting phenomena evident even in the earliest examples of liquid condensates[3,71]. Membrane bending and curvature are central to many cellular structures and processes, such as cytokinesis, endocytosis and filopodia. Membrane curvature was mostly thought to be stabilized by solid-like scaffolding proteins, especially those with curved structures such as BAR domains and the endosomal sorting complexes required for transport (ESCRTs)[43,72]. However, recent studies have reported that liquid condensates can exert elastocapillary stresses that spontaneously deform membrane surfaces into a range of shapes, such as buds and tubules[72–74] (Fig. 2e). From dimensional arguments, wetting of an elastic surface by a droplet with interfacial tension γ introduces a natural length $l_{ec} = \sqrt{\kappa/\gamma}$, known as the elastocapillary length. Physically, $1/l_{ec}$ is the largest curvature the membrane can deform into to accommodate the energetic preference for wetting (Box 2 Fig. panel **d**).

One example involves endocytic condensates that form on the membrane but are more wetting to the cytosol[43]: the membrane invaginates into the condensate, allowing the condensate to expand and maximize its contact with the cytosol, eventually leading to endocytosis of the membrane. In plants, the generation of protein storage vacuoles has been linked to how phase-separated droplets rich in storage proteins wet and deform the vacuolar membrane, eventually leading to buds

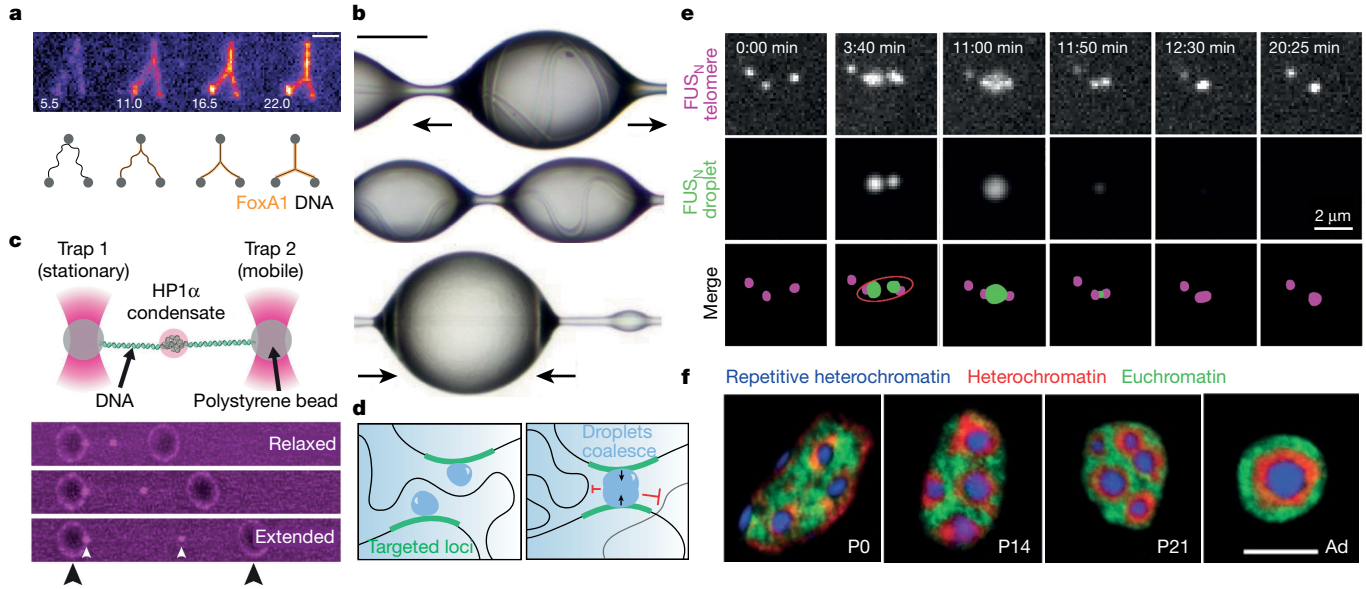

Fig. 3 | Capillary forces and genome organization. a, The transcription factor FoxA1 condenses on DNA and pulls it taut by exerting capillary forces over time (in seconds) (top) shown by the schematic (bottom). Scale bar, 2 µm. Image reproduced from ref. [86], CC BY 4.0. **b**, Images of stretching (indicated by the black arrows) in *N. edulis* capture silk showing that, under compression, the thread is spooled into the droplet (top), buckled (middle) and then stretched (bottom). Scale bar, 100 µm. Images modified with permission from ref. [87]. **c**, Schematic of optical trap experiment for stretch–relax cycles of a single unlabelled DNA molecule (top). Images showing relaxed, intermediate and extended modes of DNA in the presence of HP1α (magenta) (bottom). The white arrowheads indicate compacted HP1α–DNA, and the black arrowheads indicate the polystyrene beads. Schematic and images reproduced from ref. [88], CC BY 4.0. **d**, Schematics show restructuring of the genome through targeted droplet-mediated coalescence. Upon blue light activation, droplets (blue) nucleate at targeted genomic loci (green) (left), and they eventually coalesce, bringing these loci closer together and excluding non-targeted chromatin (black). The black arrows indicate force associated with interfacial tension, and the red inhibitory arrows indicate exclusion of chromatin. **e**, FUS$_N$ Corelet droplets (green) nucleate and grow at FUS$_N$–miRFP–TRF1-marked telomeres (pink) upon blue light activation. With light deactivation, the FUS$_N$ droplets dissolve and two telomeres coalesce into one single telomere. Images modified from ref. [91], CC BY 4.0. **f**, Inverted organization of chromatin compartments in nuclei of rods during differentiation at developmental stages postnatal day 0 (P0), P14, P21 and adult (Ad) using FISH probes detecting short interspersed nuclear elements (in green for euchromatin), long interspersed nuclear elements (in red for heterochromatin) and major satellite repeats (in blue for heterochromatin of chromocentres). Scale bar, 5 µm. Image modified from ref. [101].

(Fig. 2f) or nanotubes, depending on the wettability of the liquid to the membrane and the elastic properties of the membrane[75–77]. These examples are reminiscent of polyethylene glycol–dextran vesicle systems from the soft matter literature, in which polyethylene glycol–dextran droplets can wet the inside of a vesicle, leading to membrane deformations such as inward tubule formation, outward budding and fission[78].

Droplets wetting membranes are also present in the context of autophagosome formation—double membrane structures that are used to sequester cargo, including condensates[74]. p62, a ubiquitin-binding protein, condensates were shown to partially wet membrane sheets marked by LC3, a common marker for autophagosomes that start off as flat double membrane sheets, bending the sheets to the condensate interface. For sufficiently small condensates, droplet sequestration is trivial, as the membrane sheet always engulfs the entire condensate, forming an autophagosome. For larger condensates, engulfing part of the condensate, and hence successfully forming an autophagosome, is only possible if the interfacial tension is lower than a critical value of $\gamma_c = (\pi^2/256)\kappa/h^2$, where κ is the membrane bending modulus and h is the membrane sheet thickness (Fig. 2g) that can be identified with l_{ec}. Taking $\kappa \approx 20\ k_BT$ and $h \approx 50$ nm, we found $\gamma_c \approx 10^{-6}$ N m^{-1} comfortably in the range of typical condensates. These findings suggest that altered wetting and interfacial properties of condensates could interfere with the assembly of autophagosomal membranes, leading to deficient autophagy and thus pathology and disease.

Capillary forces and genome organization

One of the most exciting aspects of condensate capillarity is found in the context of the genome, where chromatin introduces a flexible and partially crosslinked network of DNA filaments that condensates can form in, on and around. Although the underlying interfacial physics is usually not mentioned or discussed, a number of studies provide strong support for the importance of capillary forces in organizing the 3D architecture of the genome, towards both activating gene expression[47,79–81] and repression[81–84].

Interfacial interactions between intrinsically disordered region-containing transcription factors and regions between super-enhancer-like genomic domains could mediate long-distance looping to enhance transcription. A recent study has shown that the transcription factor KLF4 wets DNA, forming local condensates along the filament whose size is set by DNA–protein interactions[85]. In this scenario, the DNA surface dictates the formation of 'microphases' that pre-wet the filament, allowing condensates to form on DNA even though the bulk concentration of KLF4 is below the saturation concentration. By condensing on DNA, transcription factors can exert capillary forces that help to remodel DNA[86]. Capillary forces exerted by condensed FoxA1 interfaces are sufficient to pull together separate DNA strands (Fig. 3a) and reel them into a FoxA1–DNA 'co-condensate'[86], reminiscent of the capillary-induced spooling of spider silk threads in droplets[87] (Fig. 3b). Similar behaviour of DNA spooling into droplets was observed with heterochromatin protein 1α (HP1α)-mediated DNA compaction[88], which was found towards the centre of the DNA molecule with both ends tethered to polystyrene beads (Fig. 3c). Repeated cycles of stretching and relaxing the DNA led to more DNA being pulled into the HP1α condensate (Fig. 3c). Together, this type of DNA-mediated surface condensation could generate capillary forces required to regulate and remodel chromatin in vivo. However, care should be taken when applying macroscopic concepts of capillarity to DNA in particular,

as the thickness of the condensate interface is probably comparable to its diameter. Nonetheless, although molecular-scale features could complicate the picture, macroscopic capillarity is a useful first approximation to access the principal physical driving forces at play.

There is far-reaching potential for new tools that probe the interplay between intracellular surface physics and genome organization to strengthen our understanding of chromatin compartmentalization and function. This includes approaches that target specific genomic loci and localize proteins prone to phase separation[47,89–91], in which the condensates that are induced to form at specific genomic loci pull these loci together via interfacial tension-mediated coalescence[47,91] (Fig. 3d,e). Here, a force is determined by droplet size and interfacial tension that is counterbalanced by chromatin elasticity, and represents another example of the elastocapillary effects described above. A recent study has used capillary forces to pull together otherwise relatively stationary telomeres, leading to their coalescence[91] (Fig. 3e). Such engineered condensates generally tend to exclude non-targeted chromatin[45,47,92] (Fig. 3d) similar to that of nucleoli and other endogenous nuclear condensates, suggesting that the default condition for condensates is to poorly wet chromatin. However, this remains an open question, with implications for the interplay between phase separation, capillarity and chromatin mechanics[30,47,92–94].

In addition to the interplay between capillarity and chromatin or DNA, the wetting behaviour of condensates on and around RNA probably has a key role for various intracellular structures, particularly nuclear condensates such as speckles and transcriptional assemblies[32], and may determine condensate size, number and morphology[95,96]. RNA molecules scaffold various RNA–ribonucleoprotein condensates, with several studies showing recruitment of RNA at condensate surfaces[97,98], suggesting that the outer peripheral regions are favourable environments for transcriptional activity[32,97]. Microphase separation has been shown to segregate the transcriptionally active and inactive domains of euchromatin, in which RNA polymerase II helps to create an interface between these domains in zebrafish nuclei[99]. RNA polymerase II tethers the RNA transcripts to chromatin, with RNA acting as an amphiphile to stabilize the euchromatin microemulsion[99].

Although most of the recent studies have focused on condensate wetting behaviour in the context of gene activation, capillary forces could also be important in the organization of heterochromatin, which are the chromatin dense and transcriptionally inactive regions of the genome probably organized in part via liquid–liquid phase separation[83,84,100]. One example lies in the 'inverted' nuclei of rods in nocturnal mammals, where heterochromatin is situated in the centre of the nucleus as opposed to its usual positioning at the nuclear periphery in conventional nuclei[101] (Fig. 3f), potentially reflecting effective relative interfacial tensions that emerge through chromatin subcompartmentalization. Future investigations should interrogate the effect of chromatin interactions on interfacial tensions in various biological contexts, including genetic programming in development and differentiation.

Surfactants for modulating intracellular capillarity

The term 'surfactant' comes from its function as a surface-active agent. In the traditional context of non-living systems, surfactants are amphiphilic molecules with both hydrophobic and hydrophilic properties, allowing them to adhere to surfaces and reduce the interfacial tensions of liquid–liquid or liquid–solid interfaces[102]. Surfactants are widely used in industry as their surface-activating properties make them useful emulsifiers, detergents and foaming agents[102]. Despite their ubiquitous commercial use, examples of surfactants on biomolecular condensates are only beginning to emerge.

One example of a natural surfactant in the cell is the proliferation marker protein Ki-67, which forms a charged polymer brush at the mitotic chromosome periphery. The short C-terminal end of the protein is bound to the chromosome, whereas the positively charged

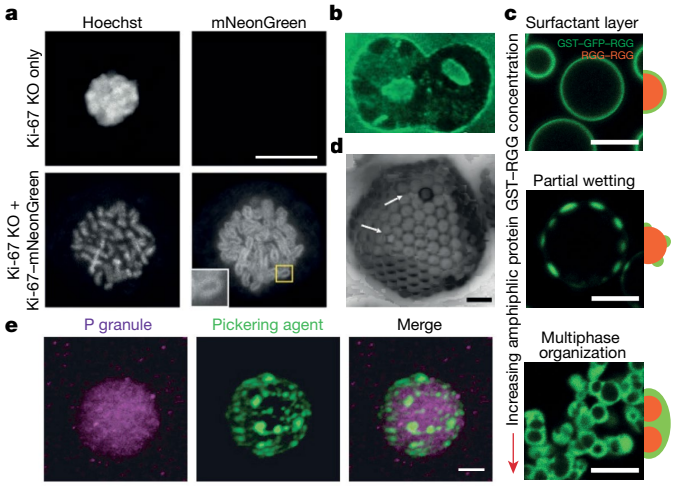

Fig. 4 | Surfactants. a, Ki-67-knockout (KO) cells with chromosomes visualized by Hoechst (top row). Ki-67-KO cells expressing Ki-67–mNeonGreen that localize to the chromosomal periphery as shown in the inset (bottom row). Scale bar, 10 µm. Image modified from ref. [103]. **b**, GFP::NO145 coats nucleoli in *X. laevis* germinal vesicles. Image modified with permission from ref. [106]. **c**, Modulating the stoichiometry and concentration of the amphiphilic GST–GFP–RGG protein (green) and RGG–RGG droplets (orange) lead to three different phase behaviours: low concentration of GST–GFP–RGG coats RGG–RGG as a thin film (top), a higher concentration of GST–GFP–RGG to RGG–RGG leads to partial engulfment (middle) and increasing the concentration of GST–GFP–RGG further leads to a multiphase system in which the GST–GFP–RGG phase completely surrounds the droplets (bottom). Scale bars, 5 µm. Image modified with permission from ref. [108]. **d**, Deformed bubbles lead to non-spherical shapes due to close packing of particles covering the surface, with the white arrows showing crumpled edges of closely packed bubbles. Scale bar, 8 µm. Image modified with permission from ref. [111]. **e**, In vitro reconstitution of a *C. elegans* P granule with PGL-3 (purple) and the Pickering agent MEG-3 (green). The merged image shows MEG-3 adsorbed onto PGL-3 condensates[114]. Scale bar, 3 µm. Image adapted with permission from ref. [114].

N-terminal domain juts into the cytoplasm to repel other chromosomes during mitosis[103] (Fig. 4a). However, the behaviour of Ki-67 at the surface is more complex than that of a traditional surfactant as it encourages chromosomes to cluster later during mitotic exit[104].

During interphase, Ki-67 localizes to the nucleolus, where it and other nucleolar proteins are enriched at the nucleolar periphery, potentially acting as nucleolar surfactants[105]. Another example is the protein NO145, which localizes to the outer surface of *X. laevis* nucleoli as a thin layer[106] (Fig. 4b). Although their functional roles remain unclear, such nucleolar surfactants could influence the flux of ribosomal components across the nucleolar interface or control nucleolar sizes by impacting their coarsening rate, either through inhibiting coalescence or Ostwald ripening.

Several studies attribute amphiphilicity to controlling and stabilizing the interfacial tension and size of biomolecular condensates. For example, surfactant-like proteins were engineered to fuse the RGG domain of LAF-1, a protein involved in P granule condensation in *C. elegans*[107], to a non-phase-separating domain[108]. Adjusting the stoichiometry and concentration of the RGG–RGG and the amphiphilic protein leads to the amphiphilic protein (1) forming a surfactant layer on the periphery of the condensate, (2) partially wetting the RGG–RGG droplet to form distinct droplets on the condensate surface, or (3) completely surrounding the core droplet leading to multiphase structures (Fig. 4c). Computational studies show that the localization of surfactant-like proteins to the surface of condensates could reflect their low valency, limiting their participation in the network of homotypic interactions, with the higher-valency proteins driving phase separation[109]. These represent minimal in vitro model systems, and related experiments

need to be performed in vivo to test how network connectivity, valency and amphiphilicity impact the stabilization, size and function of endogenous surfactant-laden condensate interfaces.

Solid particles adsorbed at interfaces can also affect the mechanics and morphology of an interface. Examples of such Pickering emulsions from traditional soft matter include deformed bubbles that are stabilized by closely packed particles at the surface[110,111] (Fig. 4d) and semi-permeable colloidosomes[112]. This Pickering-type behaviour reflects an interesting physical result: as long as a particle partially wets a droplet, then it is always energetically favourable for the particle to straddle the surface (Box 2 Fig. panel **f**)[112,113].

A recent study has characterized an RNA-binding protein, MEG-3, of *C. elegans*, as a Pickering agent that adsorbs onto the P granule (formed by PGL-3) interface in vivo and in vitro[114] (Fig. 4e). Assuming the MEG-3 clusters are of a typical size $R \approx 50$ nm and $\gamma \approx 10^{-5}$ N m^{-1}, we can use the equation in Box 2 panel **f** to estimate an upper bound for the Pickering stabilization energy to be approximately 20 $k_B T$, which represents substantial adhesion. The MEG-3 solid-like clusters stabilize PGL-3 emulsion and result in reduced PGL-3 coarsening kinetics during the oocyte-to-zygote transition. Another study has shown that soluble tubulin subunits preferentially localize to stress granule interfaces in a manner consistent with the Pickering picture, as long as one accounts for a finite interfacial thickness[54]. More examples of intracellular Pickering behaviour are likely to be found; they may regulate the exchange and/or sequestration of biomolecules within condensates by modulating interfacial properties[114]. Moreover, with non-spherical particles, or spherical particles on surfaces with more complex curvature, a distorted contact line can cause them to move[115,116], providing a driving force for self-assembly of biological particles on condensate surfaces.

Outlook

In this Perspective article, we have discussed the importance of capillary phenomena in various intracellular processes, including ribosome production, endocytosis and genome organization, among others (Figs. 1–4). In these examples, the surfaces of biomolecular condensates have a dominant role, which we have interpreted through the lens of capillary physics (Box 2). The plethora of examples presented here provide strong evidence that capillary forces are prevalent within living cells and are important for cell morphology, structure and function. One area for future work concerns condensates that manifest at the nanoscale, where modifications to the framework of macroscopic capillarity may be needed. Indeed, as the ratio of the molecular size a to the condensate size R becomes less negligible (Box 2 Fig. panels **a**,**b**), one might need to consider the interface as a transition region of finite thickness[54,117]. This highlights how biomolecular condensates present opportunities for the application of classical physics concepts within living cells, but also the potential for the complex, multicomponent and multiscale organization of the cell to yield new principles of interfacial physics. Capillarity thus represents an exciting new frontier of intracellular force generation, analogous to the activity of molecular motors, and can likewise be harnessed for functional intracellular motion and structural organization.

1. Shin, Y. & Brangwynne, C. P. Liquid phase condensation in cell physiology and disease. *Science* **357**, eaaf4382 (2017).
2. Banani, S. F., Lee, H. O., Hyman, A. A. & Rosen, M. K. Biomolecular condensates: organizers of cellular biochemistry. *Nat. Rev. Mol. Cell Biol.* **18**, 285–298 (2017).
3. Brangwynne, C. P. et al. Germline P granules are liquid droplets that localize by controlled dissolution/condensation. *Science* **324**, 1729–1732 (2009).
4. Seydoux, G. The P granules of *C. elegans*: a genetic model for the study of RNA–protein condensates. *J. Mol. Biol.* **430**, 4702–4710 (2018).
5. Feric, M. et al. Coexisting liquid phases underlie nucleolar subcompartments. *Cell* **165**, 1686–1697 (2016).
Nucleoli are multiphase liquid condensates whose core–shell organization is governed by relative interfacial tensions.
6. Frottin, F. et al. The nucleolus functions as a phase-separated protein quality control compartment. *Science* **365**, 342–347 (2019).
7. Wheeler, J. R., Matheny, T., Jain, S., Abrisch, R. & Parker, R. Distinct stages in stress granule assembly and disassembly. *eLife* **5**, e18413 (2016).
8. Freeman Rosenzweig, E. S. et al. The eukaryotic CO_2-concentrating organelle is liquid-like and exhibits dynamic reorganization. *Cell* **171**, 148–162.e19 (2017).
9. Kilic, S. et al. Phase separation of 53BP1 determines liquid-like behavior of DNA repair compartments. *EMBO J.* **38**, e101379 (2019).
10. Li, P. et al. Phase transitions in the assembly of multivalent signalling proteins. *Nature* **483**, 336–340 (2012).
11. Martin, E. W. et al. Valence and patterning of aromatic residues determine the phase behavior of prion-like domains. *Science* **367**, 694–699 (2020).
12. Zarzar, L. D. et al. Dynamically reconfigurable complex emulsions via tunable interfacial tensions. *Nature* **518**, 520–524 (2015).
13. Marthelot, J., Strong, E. F., Reis, P. M. & Brun, P.-T. Designing soft materials with interfacial instabilities in liquid films. *Nat. Commun.* **9**, 4477 (2018).
14. Duprat, C., Aristoff, J. M. & Stone, H. A. Dynamics of elastocapillary rise. *J. Fluid Mech.* **679**, 641–654 (2011).
15. Roman, B. & Bico, J. Elasto-capillarity: deforming an elastic structure with a liquid droplet. *J. Phys. Condens. Matter* **22**, 493101 (2010).
16. Steinberg, M. S. Adhesion in development: an historical overview. *Dev. Biol.* **180**, 377–388 (1996).
17. Hayashi, T. & Carthew, R. W. Surface mechanics mediate pattern formation in the developing retina. *Nature* **431**, 647–652 (2004).
18. Rubinstein, M. & Colby, R. H. *Polymer Physics* (Oxford Univ. Press, 2003).
19. Aarts, D. G. A. L., Schmidt, M. & Lekkerkerker, H. N. W. Direct visual observation of thermal capillary waves. *Science* **304**, 847–850 (2004).
20. Dill, K. & Bromberg, S. *Molecular Driving Forces: Statistical Thermodynamics in Biology, Chemistry, Physics, and Nanoscience* (Garland Science, 2010).
21. Mao, S., Kuldinow, D., Haataja, M. P. & Košmrlj, A. Phase behavior and morphology of multicomponent liquid mixtures. *Soft Matter* **15**, 1297–1311 (2019).
22. Cahn, J. W. & Hilliard, J. E. Free energy of a nonuniform system. I. Interfacial free energy. *J. Chem. Phys.* **28**, 258–267 (1958).
23. Berry, J., Brangwynne, C. P. & Haataja, M. Physical principles of intracellular organization via active and passive phase transitions. *Rep. Prog. Phys.* **81**, 046601 (2018).
24. Molliex, A. et al. Phase separation by low complexity domains promotes stress granule assembly and drives pathological fibrillization. *Cell* **163**, 123–133 (2015).
25. Lin, Y., Protter, D. S. W., Rosen, M. K. & Parker, R. Formation and maturation of phase-separated liquid droplets by RNA-binding proteins. *Mol. Cell* **60**, 208–219 (2015).
26. Zhang, H. et al. RNA controls polyQ protein phase transitions. *Mol. Cell* **60**, 220–230 (2015).
27. Putnam, A., Cassani, M., Smith, J. & Seydoux, G. A gel phase promotes condensation of liquid P granules in *Caenorhabditis elegans* embryos. *Nat. Struct. Mol. Biol.* **26**, 220–226 (2019).
28. Patel, A. et al. A liquid-to-solid phase transition of the ALS protein FUS accelerated by disease mutation. *Cell* **162**, 1066–1077 (2015).
29. Eggers, J., Lister, J. R. & Stone, H. A. Coalescence of liquid drops. *J. Fluid Mech.* **401**, 293–310 (1999).
30. Rosowski, K. A. et al. Elastic ripening and inhibition of liquid–liquid phase separation. *Nat. Phys.* **16**, 422–425 (2020).
31. Sanders, D. W. et al. Competing protein–RNA interaction networks control multiphase intracellular organization. *Cell* **181**, 306–324.e28 (2020).
32. Fei, J. et al. Quantitative analysis of multilayer organization of proteins and RNA in nuclear speckles at super resolution. *J. Cell Sci.* **130**, 4180–4192 (2017).
33. Kaur, T. et al. Sequence-encoded and composition-dependent protein–RNA interactions control multiphasic condensate morphologies. *Nat. Commun.* **12**, 872 (2021). **A ternary system of protein and RNA is used to show that the wetting morphologies of the resulting biphasic condensates depend strongly on component stoichiometry and intermolecular interaction hierarchy.**
34. Fisher, R. S. & Elbaum-Garfinkle, S. Tunable multiphase dynamics of arginine and lysine liquid condensates. *Nat. Commun.* **11**, 4628 (2020).
35. Boeynaems, S. et al. Spontaneous driving forces give rise to protein–RNA condensates with coexisting phases and complex material properties. *Proc. Natl Acad. Sci. USA* **116**, 7889–7898 (2019).
36. Simon, J. R., Carroll, N. J., Rubinstein, M., Chilkoti, A. & López, G. P. Programming molecular self-assembly of intrinsically disordered proteins containing sequences of low complexity. *Nat. Chem.* **9**, 509–515 (2017).
37. Gall, J. G., Bellini, M., Wu, Z. & Murphy, C. Assembly of the nuclear transcription and processing machinery: Cajal bodies (coiled bodies) and transcriptosomes. *Mol. Biol. Cell* **10**, 4385–4402 (1999).
38. Pena, E., Berciano, M. T., Fernandez, R., Ojeda, J. L. & Lafarga, M. Neuronal body size correlates with the number of nucleoli and Cajal bodies, and with the organization of the splicing machinery in rat trigeminal ganglion neurons. *J. Comp. Neurol.* **430**, 250–263 (2001).
39. Caragine, C. M., Haley, S. C. & Zidovska, A. Surface fluctuations and coalescence of nucleolar droplets in the human cell nucleus. *Phys. Rev. Lett.* **121**, 148101 (2018).
40. Ijavi, M. et al. Surface tensiometry of phase separated protein and polymer droplets by the sessile drop method. *Soft Matter* **17**, 1655–1662 (2021).
41. Jawerth, L. M. et al. Salt-dependent rheology and surface tension of protein condensates using optical traps. *Phys. Rev. Lett.* **121**, 258101 (2018).
42. Wang, H., Kelley, F. M., Milovanovic, D., Schuster, B. S. & Shi, Z. Surface tension and viscosity of protein condensates quantified by micropipette aspiration. *Biophys. Rep.* **1**, 100011 (2021).
43. Bergeron-Sandoval, L.-P. et al. Endocytic proteins with prion-like domains form viscoelastic condensates that enable membrane remodeling. *Proc. Natl Acad. Sci. USA* **118**, e2113789118 (2021).

44. Shin, Y. et al. Spatiotemporal control of intracellular phase transitions using light-activated optoDroplets. *Cell* **168**, 159–171.e14 (2017).
45. Bracha, D. et al. Mapping local and global liquid phase behavior in living cells using photo-oligomerizable seeds. *Cell* **175**, 1467–1480.e13 (2018).
46. Dine, E., Gil, A. A., Uribe, G., Brangwynne, C. P. & Toettcher, J. E. Protein phase separation provides long-term memory of transient spatial stimuli. *Cell Syst.* **6**, 655–663.e5 (2018).
47. Shin, Y. et al. Liquid nuclear condensates mechanically sense and restructure the genome. *Cell* **175**, 1481–1491.e13 (2018). **Nuclear condensates exert capillary forces on targeted genomic loci to pull them together while excluding the rest of the neighbouring genome.**
48. Narayanan, A. et al. A first order phase transition mechanism underlies protein aggregation in mammalian cells. *eLife* **8**, e39695 (2019).
49. Shimobayashi, S., Ronceray, P., Sanders, D. W., Haataja, M. & Brangwynne, C. P. Nucleation landscape of biomolecular condensates. *Nature* **599**, 503–506 (2021).
50. Kashchiev, D. *Nucleation* (Elsevier, 2000).
51. Wiegand, T. & Hyman, A. A. Drops and fibers—how biomolecular condensates and cytoskeletal filaments influence each other. *Emerg. Top. Life Sci.* **4**, 247–261 (2020).
52. Su, X. et al. Phase separation of signaling molecules promotes T cell receptor signal transduction. *Science* **352**, 595–599 (2016).
53. Feric, M. & Brangwynne, C. P. A nuclear F-actin scaffold stabilizes ribonucleoprotein droplets against gravity in large cells. *Nat. Cell Biol.* **15**, 1253–1259 (2013).
54. Böddeker, T. J. et al. Non-specific adhesive forces between filaments and membraneless organelles. *Nat. Phys.* **18**, 571–578 (2022). **Tubulin subunits and microtubules adhere to condensate interfaces in a manner consistent with a Pickering model that accounts for the finite interfacial thickness.**
55. Sanchez, T., Chen, D. T. N., DeCamp, S. J., Heymann, M. & Dogic, Z. Spontaneous motion in hierarchically assembled active matter. *Nature* **491**, 431–434 (2012).
56. Kumar, N., Zhang, R., de Pablo, J. J. & Gardel, M. L. Tunable structure and dynamics of active liquid crystals. *Sci. Adv.* **4**, eaat7779 (2018).
57. Weirich, K. L. et al. Liquid behavior of cross-linked actin bundles. *Proc. Natl Acad. Sci. USA* **114**, 2131–2136 (2017).
58. Zwicker, D., Seyboldt, R., Weber, C. A., Hyman, A. A. & Jülicher, F. Growth and division of active droplets provides a model for protocells. *Nat. Phys.* **13**, 408–413 (2017).
59. Weirich, K. L., Dasbiswas, K., Witten, T. A., Vaikuntanathan, S. & Gardel, M. L. Self-organizing motors divide active liquid droplets. *Proc. Natl Acad. Sci. USA* **116**, 11125–11130 (2019).
60. Jiang, H. et al. Phase transition of spindle-associated protein regulate spindle apparatus assembly. *Cell* **163**, 108–122 (2015).
61. King, M. R. & Petry, S. Phase separation of TPX2 enhances and spatially coordinates microtubule nucleation. *Nat. Commun.* **11**, 270 (2020).
62. Hernández-Vega, A. et al. Local nucleation of microtubule bundles through tubulin concentration into a condensed tau phase. *Cell Rep.* **20**, 2304–2312 (2017). **Microtubules nucleate from tau condensates, resulting in a wetted network of microtubule bundles, the wettability of which can be tuned by heparin.**
63. Siahaan, V. et al. Kinetically distinct phases of tau on microtubules regulate kinesin motors and severing enzymes. *Nat. Cell Biol.* **21**, 1086–1092 (2019).
64. Jijumon, A. S. et al. Lysate-based pipeline to characterize microtubule-associated proteins uncovers unique microtubule behaviours. *Nat. Cell Biol.* **24**, 253–267 (2022).
65. Setru, S. U. et al. A hydrodynamic instability drives protein droplet formation on microtubules to nucleate branches. *Nat. Phys.* **17**, 493–498 (2021). **A Rayleigh–Plateau instability with condensed TPX2 on microtubules results in droplets that serve as reaction hubs to form microtubule branches.**
66. Petry, S., Groen, A. C., Ishihara, K., Mitchison, T. J. & Vale, R. D. Branching microtubule nucleation in *Xenopus* egg extracts mediated by augmin and TPX2. *Cell* **152**, 768–777 (2013).
67. Valentine, M. T., Fordyce, P. M., Krzysiak, T. C., Gilbert, S. P. & Block, S. M. Individual dimers of the mitotic kinesin motor Eg5 step processively and support substantial loads in vitro. *Nat. Cell Biol.* **8**, 470–476 (2006).
68. Bäuerlein, F. J. B. et al. In situ architecture and cellular interactions of polyQ inclusions. *Cell* **171**, 179–187.e10 (2017).
69. Fisher, R. S., Jimenez, R. M., Soto, E., Kalev, D. & Elbaum-Garfinkle, S. An apparent core/shell architecture of polyQ aggregates in the aging *Caenorhabditis elegans* neuron. *Protein Sci.* **30**, 1482–1486 (2021).
70. Yu, H. et al. HSP70 chaperones RNA-free TDP-43 into anisotropic intranuclear liquid spherical shells. *Science* **371**, eabb4309 (2021).
71. Updike, D. L., Hachey, S. J., Kreher, J. & Strome, S. P granules extend the nuclear pore complex environment in the *C. elegans* germ line. *J. Cell Biol.* **192**, 939–948 (2011).
72. Yuan, F. et al. Membrane bending by protein phase separation. *Proc. Natl Acad. Sci. USA* **118**, e2017435118 (2021).
73. Kusumaatmaja, H. & Lipowsky, R. Droplet-induced budding transitions of membranes. *Soft Matter* **7**, 6914–6919 (2011).
74. Agudo-Canalejo, J. et al. Wetting regulates autophagy of phase-separated compartments and the cytosol. *Nature* **591**, 142–146 (2021). **Autophagosomes sequester p62-rich condensates by wrapping around them via a wetting interaction; successful autophagy depends on condensate size, interfacial tension and membrane stiffness.**
75. Kusumaatmaja, H. et al. Wetting of phase-separated droplets on plant vacuole membranes leads to a competition between tonoplast budding and nanotube formation. *Proc. Natl Acad. Sci. USA* **118**, e2024109118 (2021). **Wetting of phase-separated droplets on plant vacuolar membranes can lead to membrane budding or the formation of membrane nanotubes depending on the contact angle and the membrane spontaneous curvature.**
76. Feeney, M., Kittelmann, M., Menassa, R., Hawes, C. & Frigerio, L. Protein storage vacuoles originate from remodeled preexisting vacuoles in Arabidopsis thaliana. *Plant Physiol.* **177**, 241–254 (2018).
77. Zheng, H. & Staehelin, L. A. Protein storage vacuoles are transformed into lytic vacuoles in root meristematic cells of germinating seedlings by multiple, cell type-specific mechanisms. *Plant Physiol.* **155**, 2023–2035 (2011).
78. Dimova, R. & Lipowsky, R. Lipid membranes in contact with aqueous phases of polymer solutions. *Soft Matter* **8**, 6409–6415 (2012).
79. Wei, M.-T. et al. Nucleated transcriptional condensates amplify gene expression. *Nat. Cell Biol.* **22**, 1187–1196 (2020).
80. Sabari, B. R. et al. Coactivator condensation at super-enhancers links phase separation and gene control. *Science* **361**, eaar3958 (2018).
81. Gibson, B. A. et al. Organization of chromatin by intrinsic and regulated phase separation. *Cell* **179**, 470–484.e21 (2019).
82. Tatavosian, R. et al. Nuclear condensates of the Polycomb protein chromobox 2 (CBX2) assemble through phase separation. *J. Biol. Chem.* **294**, 1451–1463 (2019).
83. Strom, A. R. et al. Phase separation drives heterochromatin domain formation. *Nature* **547**, 241–245 (2017).
84. Larson, A. G. et al. Liquid droplet formation by HP1α suggests a role for phase separation in heterochromatin. *Nature* **547**, 236–240 (2017).
85. Morin, J. A. et al. Sequence-dependent surface condensation of a pioneer transcription factor on DNA. *Nat. Phys.* **18**, 271–276 (2022).
86. Quail, T. et al. Force generation by protein–DNA co-condensation. *Nat. Phys.* **17**, 1007–1012 (2021). **The condensed transcription factor FoxA1 wets DNA and regulates its tension by allowing slack DNA to spool into FoxA1 droplets.**
87. Elettro, H., Neukirch, S., Vollrath, F. & Antkowiak, A. In-drop capillary spooling of spider capture thread inspires hybrid fibers with mixed solid–liquid mechanical properties. *Proc. Natl Acad. Sci. USA* **113**, 6143–6147 (2016).
88. Keenen, M. M. et al. HP1 proteins compact DNA into mechanically and positionally stable phase separated domains. *eLife* **10**, e64563 (2021).
89. Gao, Y., Han, M., Shang, S., Wang, H. & Qi, L. S. Interrogation of the dynamic properties of higher-order heterochromatin using CRISPR/dCas9. *Mol. Cell* **81**, 4287–4299.e5 (2021).
90. Wang, H. et al. CRISPR-mediated programmable 3D genome positioning and nuclear organization. *Cell* **175**, 1405–1417.e14 (2018).
91. Jack, A. et al. Compartmentalization of telomeres through DNA-scaffolded phase separation. *Dev. Cell* **57**, 277–290.e9 (2022).
92. Lee, D. S. W., Wingreen, N. S. & Brangwynne, C. P. Chromatin mechanics dictates subdiffusion and coarsening dynamics of embedded condensates. *Nat. Phys.* **17**, 531–538 (2021).
93. Ronceray, P., Sheng, M., Košmrlj, A. & Haataja, M. P. Liquid demixing in elastic networks: cavitation, permeation, or size selection?. *EPL* **137**, 67001 (2022).
94. Zhang, Y., Lee, D. S. W., Meir, Y., Brangwynne, C. P. & Wingreen, N. S. Mechanical frustration of phase separation in the cell nucleus by chromatin. *Phys. Rev. Lett.* **126**, 258102 (2021).
95. Snead, W. T. et al. Membrane surfaces regulate assembly of ribonucleoprotein condensates. *Nat. Cell Biol.* **24**, 461–470 (2022).
96. Cochard, A. et al. RNA at the surface of phase-separated condensates impacts their size and number. *Biophys. J.***121**, 1675–1690 (2022).
97. Boisvert, F. M., Hendzel, M. J. & Bazett-Jones, D. P. Promyelocytic leukemia (PML) nuclear bodies are protein structures that do not accumulate RNA. *J. Cell Biol.* **148**, 283–292 (2000).
98. Tauber, D. et al. Modulation of RNA condensation by the DEAD-box protein eIF4A. *Cell* **180**, 411–426.e16 (2020).
99. Hilbert, L. et al. Transcription organizes euchromatin via microphase separation. *Nat. Commun.* **12**, 1360 (2021).
100. Plys, A. J. et al. Phase separation of Polycomb-repressive complex 1 is governed by a charged disordered region of CBX2. *Genes Dev.* **33**, 799–813 (2019).
101. Falk, M. et al. Heterochromatin drives compartmentalization of inverted and conventional nuclei. *Nature* **570**, 395–399 (2019).
102. De, S., Malik, S., Ghosh, A., Saha, R. & Saha, B. A review on natural surfactants. *RSC Adv.* **5**, 65757–65767 (2015).
103. Cuylen, S. et al. Ki-67 acts as a biological surfactant to disperse mitotic chromosomes. *Nature* **535**, 308–312 (2016).
104. Cuylen-Haering, S. et al. Chromosome clustering by Ki-67 excludes cytoplasm during nuclear assembly. *Nature* **587**, 285–290 (2020).
105. Stenström, L. et al. Mapping the nucleolar proteome reveals a spatiotemporal organization related to intrinsic protein disorder. *Mol. Syst. Biol.* **16**, e9469 (2020).
106. Brangwynne, C. P., Mitchison, T. J. & Hyman, A. A. Active liquid-like behavior of nucleoli determines their size and shape in *Xenopus laevis* oocytes. *Proc. Natl Acad. Sci. USA* **108**, 4334–4339 (2011).
107. Elbaum-Garfinkle, S. et al. The disordered P granule protein LAF-1 drives phase separation into droplets with tunable viscosity and dynamics. *Proc. Natl Acad. Sci. USA* **112**, 7189–7194 (2015).
108. Kelley, F. M., Favetta, B., Regy, R. M., Mittal, J. & Schuster, B. S. Amphiphilic proteins coassemble into multiphasic condensates and act as biomolecular surfactants. *Proc. Natl Acad. Sci. USA* **118**, e2109967118 (2021). **Amphiphilic surfactant-like proteins regulate the size and multiphasic wetting morphologies of condensates in a concentration-dependent and sequence-dependent manner.**
109. Sanchez-Burgos, I., Joseph, J. A., Collepardo-Guevara, R. & Espinosa, J. R. Size conservation emerges spontaneously in biomolecular condensates formed by scaffolds and surfactant clients. *Sci. Rep.* **11**, 15241 (2021).
110. Subramaniam, A. B., Abkarian, M., Mahadevan, L. & Stone, H. A. Colloid science: non-spherical bubbles. *Nature* **438**, 930 (2005).
111. Abkarian, M. et al. Dissolution arrest and stability of particle-covered bubbles. *Phys. Rev. Lett.* **99**, 188301 (2007).
112. Dinsmore, A. D. et al. Colloidosomes: selectively permeable capsules composed of colloidal particles. *Science* **298**, 1006–1009 (2002).
113. Binks, B. P. & Clint, J. H. Solid wettability from surface energy components: relevance to Pickering emulsions. *Langmuir* **18**, 1270–1273 (2002).
114. Folkmann, A. W., Putnam, A., Lee, C. F. & Putnam, G. Pickering stabilization of a dynamic intracellular emulsion. *Science* **373**, 1218–1224 (2021). **MEG-3 assemblies adhere to the interface of P granules and slow their coarsening through a Pickering effect, thereby stabilizing the emulsion of P granules.**

115. Würger, A. Curvature-induced capillary interaction of spherical particles at a liquid interface. *Phys. Rev. E* **74**, 041402 (2006).
116. Cavallaro, M. Jr, Botto, L., Lewandowski, E. P., Wang, M. & Stebe, K. J. Curvature-driven capillary migration and assembly of rod-like particles. *Proc. Natl Acad. Sci. USA* **108**, 20923–20928 (2011).
117. Boruvka, L. & Neumann, A. W. Generalization of the classical theory of capillarity. *J. Chem. Phys.* **66**, 5464–5476 (1977).

Acknowledgements We thank members of our laboratories for helpful discussions; and M. Haataja for helpful comments on the manuscript. We acknowledge support from the Howard Hughes Medical Institute, the Princeton Biomolecular Condensate Program, and grants from the Princeton Center for Complex Materials, a MRSEC (NSF DMR-2011750), and the AFOSR MURI 'Uncovering and applying the interfacial design principles of multiphasic natural and synthetic organelles' (FA9550-20-1-0241). B.G. acknowledges the PD Soros Foundation. Both B.G. and Y.K. are supported by the NSF GRFP (DGE-2039656).

Author contributions B.G., Y.K., H.A.S. and C.P.B. wrote the manuscript with input from J.W.S. and S.P. All authors contributed to conceptualization, design and editing of the manuscript.

Competing interests C.P.B. is a founder of and consultant for Nereid Therapeutics. All other authors declare no competing interests.

Additional information
Correspondence and requests for materials should be addressed to Howard A. Stone or Clifford P. Brangwynne.
Peer review information *Nature* thanks the anonymous reviewers for their contribution to the peer review of this work.
Reprints and permissions information is available at http://www.nature.com/reprints.
Publisher's note Springer Nature remains neutral with regard to jurisdictional claims in published maps and institutional affiliations.